Journal of Hazardous Materials 189 (2011) 329–335

Contents lists available at ScienceDirect

Journal of Hazardous Materials

journal homepage: www.elsevier.com/locate/jhazmat

Synthesis and photo-degradation application of WO_3/TiO_2 hollow spheres

Kezhen Lv, Jie Li*, Xiaoxia Qing, Wenzhang Li, Qiyuan Chen

Key Laboratory of Resource Chemistry of Nonferrous Metals, Ministry of Education, China, College of Chemistry and Chemical Engineering, Central South University, Changsha 410083, China

ARTICLE INFO

Article history:
Received 26 September 2010
Received in revised form 15 February 2011
Accepted 15 February 2011
Available online 22 February 2011

Keywords:
Carbon sphere template
Hollow sphere
WO_3/TiO_2
Photo-degradation
Methylene blue

ABSTRACT

A WO_3/TiO_2 composite, hollow-sphere photocatalyst with average diameter of 320 nm and shell thickness of 50 nm was successfully prepared using a template method. UV–vis diffuse reflectance spectra illustrated that the main absorption edges of the WO_3/TiO_2 hollow spheres were red-shifted compared to the TiO_2 hollow spheres, indicating an extension of light absorption into the visible region of the composite photocatalyst. The WO_3 and TiO_2 phases were confirmed by X-ray diffraction analysis. BET isotherms revealed that the specific surface area and average pore diameter of the hollow spheres were 40.95 m^2/g and 19 nm, respectively. Photocatalytic experiments indicate that 78% MB was degraded by WO_3/TiO_2 hollow spheres under visible light within 80 min. Under the same conditions, only 24% MB can be photodegraded by TiO_2. The photocatalytic mineralization of MB, catalyzed by TiO_2 and WO_3/TiO_2, proceeded at a significantly higher rate under UV irradiation than that under visible light, and more significant was the increase in the apparent rate constant with the WO_3/TiO_2 composite semiconductor material which was 3.2- and 3.5-fold higher than with the TiO_2 material under both UV and visible light irradiation. The increased photocatalytic activity of the coupled nanocomposites was attributed to photoelectron/hole separation efficiency and the extension of the wavelength range of photoexcitation.

1. Introduction

Semiconductor photocatalysts have attracted enormous attention because of their wide applications in environmental purification, such as air and water purification, and organic pollutant degradation [1–4]. Among the oxide semiconductor photocatalysts available, titanium dioxide has proven to be the most widely used one for environmental catalysis because it has various merits, such as excellent photocatalytic activity, low cost, nontoxicity, and chemical and biological inertness [5,6]. However, TiO_2 has two major disadvantages that restrict it from being widely used in practical applications: (1) the rapid recombination of photogenerated electron (e_{cb}^-)/hole (h_{VB}^+) pairs, which significantly reduces photocatalytic efficiency [7]; and (2) the location of its light response region in the UV region, which accounts for only about 5% of the energy of sunlight.

Considerable efforts have been made to prevent the recombination of charge carriers in the semiconductor and improve the photocatalytic efficiency of TiO_2, such as doping with metal ions, especially transition metal ions into the TiO_2 lattice [8], deposition of noble metals [9], dye photosensitization on the TiO_2 surface [10,11], and coupling with other semiconductors, such as ZnO–TiO_2 [12], V_2O_5–TiO_2 [13], ZrO_2–TiO_2 [14,15], CdS–TiO_2 [16,17] and WO_3–TiO_2 [18–22]. Among the oxide semiconductors, coupling TiO_2 with WO_3 has been the subject of intensive investigations during the last 15 years [18,22] as an approach that for achieving an efficient charge separation and improving the photocatalytic properties of TiO_2.

Morphology and microstructures play an important role in the photocatalytic activity of titania. Many studies concerning the new structures of titania, such as titanium dioxide nanowires, nanorods, nanotubes [23,24], and so on, have been undertaken. Recently, the preparation of titania hollow microspheres has also attracted much attention because of their large surface area, low density, and highly efficient light-harvesting abilities [7,25]. Despite the fact that many papers have focused on the fabrication of nano- and micro-scale hollow spheres, most of these studies focus on the synthesis and morphology of pure phase titania.

Several synthetic approaches have been employed for preparing mixed metal–oxide systems with core–shell morphology. In comparison to other particles, hollow spheres can be widely used in several applications, such as drug delivery, protection of light-sensitive biological molecules, controlled release of various substances, nano-reactors, and paints and fillers, among others. Hollow balls have many advantages compared to porous particles because of the relatively low density of the former compared to the latter.

In the present work, hollow spheres composed of mixed WO_3/TiO_2 metal oxide shells were synthesized using colloidal carbon spheres as the template. The aim of this study was to design and

* Corresponding author. Tel.: +86 731 8887 7364; fax: +86 731 8887 9616.
E-mail address: lijieliu@mail.csu.edu.cn (J. Li).

0304-3894/$ – see front matter © 2011 Elsevier B.V. All rights reserved.
doi:10.1016/j.jhazmat.2011.02.038

construct WO_3/TiO_2 hollow spheres that can be effectively applied in air/water purification and organic pollutant degradation.

2. Experimental

2.1. Materials

All reagents were of analytical grade and were subjected to no further treatment. Tetrabutyl titanate, $Ti(OBu)_4$ (Sinopharm Chemical Reagent Co., Ltd.) was used as the starting material. Glucose, D-(+)-$C_6H_{12}O_6$ (Sinopharm Chemical Reagent Co., Ltd.), absolute ethanol, CH_3CH_2OH (Sinopharm Chemical Reagent Co., Ltd.) and ammonium metatungstate, $(NH_4)_6W_7O_{24}{\cdot}6H_2O$ (Sinopharm Chemical Reagent Co., Ltd.) were used as received. The water used throughout was deionized and doubly distilled.

2.2. Preparation of carbon spheres

In a typical experiment [26], 12 g of glucose was dissolved in 80 mL of water to form a solution. The solution was then sealed in a 100 mL Teflon-lined autoclave and maintained at 180 °C for 4 h. The products were centrifuged (5000 r/min), washed, and dispersed in water for five cycles, after which they were centrifuged, washed, and redispersed in ethanol for five cycles. The carbon spheres were then dried at 80 °C for 2 h under a vacuum.

2.3. Synthesis of WO_3/TiO_2 core–shell particles

The starting solution was prepared by mixing 1 mL $Ti(OBu)_4$ and 20 mL ethanol, followed by the addition of 0.06 g ammonium metatungstate. After stirring at 40 °C for 30 min, a sample of 0.1 g colloidal carbon spheres, as prepared in Section 2.1, was added to the reaction media, which was then stirred vigorously for 1 h. When the mixture had cooled to room temperature, it was centrifuged, washed, and dispersed in ethanol for five cycles. The mixture was aged in air at room temperature for 12 h and dried at 60 °C in a vacuum oven. To fabricate the 4.5 wt% WO_3/TiO_2 composite particles, the mixture was heated at a rate of 2 K/min from room temperature and kept at 550 °C for 4 h in muffle furnace. For comparison, the same procedure was followed to produce TiO_2 hollow spheres without the addition of ammonium metatungstate.

2.4. Structural characterization

The structural properties were determined by an X-ray diffractometer (XRD, XD-3A, Shimadazu Corporation, Japan) using graphite monochromatic copper radiation (Cu-Kα) at 40 kV and 30 mA over the 2 h range 20–80°. The Scherrer equation (Eq. (1)) was applied to estimate the average crystallite sizes of WO_3/TiO_2 samples [14]:

$$D = \frac{k\lambda}{\beta \cos\theta} \tag{1}$$

where D, λ, β are the crystallite size, the X-ray wavelength, the half-height width of the diffraction peak of anatase titania (1 0 1) and $k = 0.89$ is a coefficient. The hollow particles were characterized by transmission electron microscopy (TEM, JEM2000EX, Japan). The morphologies of WO_3/TiO_2 and TiO_2 particles were observed by a scanning electron microscope (SEM, JSM-5600LV, Japan). BET surface area measurements were carried out via N_2 adsorption at 77 K using an ASAP2020 instrument based on adsorption data in the partial pressure (P/P_0) range of 0.01–0.99. Infrared spectra were obtained using a Nicolet 6700 FT-IR spectrometer (Thermo Fisher, America). Spectra over the 4000–475 cm^{-1} range were obtained by the co-addition of 256 scans with a resolution of 4 cm^{-1} and a mirror velocity of 0.6329 cm/s. Spectra were co-added to improve the signal to noise ratio. The UV–vis absorption spectra of the WO_3/TiO_2 hollow spheres were collected using a Shimadzu UV-2100 instrument equipped with an integrating sphere to characterize the spectral features of the photocatalyst samples and to determine semiconductor band-gap energies. The indirect band gap energies of the two titania samples can be estimated from a plot of $(ahv)^{1/2}$ versus photon energy (hv) by the following equation (Eq. (2)) near the band edge [27]:

$$ahv = B_i(hv - E_g)^2 \tag{2}$$

Here, a, v, E_g and B_i are absorption coefficient, light frequency, band gap, absorption constant. The E_g values determined by extrapolating the linear region of the plot to $hv = 0$.

2.5. Photo-degradation application of WO_3/TiO_2

In the photocatalytic experiments, 5 mg of WO_3/TiO_2 hollow spheres were dispersed into 200 mL of an aqueous methylene blue (MB) solution (10 mg/L, initial PH 7, 25 °C). Prior to photooxidation, the suspension was magnetically stirred (300 rpm) in a dark condition for 30 min. The aqueous suspension containing MB and photocatalyst were irradiated under UV and visible light. The photocatalytic reactor used is a cylindrical concentric Pyrex-quartz tubular reactor. In the reactor system, six sets of 365 nm, 6 W UV lamps (FL6BLB, Sankyo, Japan) for UV irradiation or a 110 W high-pressure sodium lamp (Institute of Electrical Light Source, Beijing) for visible light irradiation were used to allow independent control of the on/off status of each lamp. The UV lamp was positioned inside the cylindrical Pyrex vessel surrounded by a circulating water jacket (Pyrex) to cool the reaction solution. The visible light lamp was located 10 cm above the surface of the liquid in the reactor; a 400 nm cut-off glass filter was used to remove the radiation in the UV region emitted by the visible light lamps. The photon flux in the visible light region at the surface of the liquid was 7 mW/cm^2, determined with a Radiometer (FZ-A, Beijing) fitted with 420 nm sensor. The photon flux in the UV light region at the external wall of the quartz tube was 135 μW/cm^2, determined with a Radiometer (UV-A, Beijing) fitted with 365 nm sensor. At the given time intervals (5 and 15 min), analytical samples were taken from the suspension and immediately centrifuged at 80 rps for 10 min. MB concentration was analyzed by a UV–vis spectroscopy (Shimadzu UV-2100). The degradation rate can be calculated using Eq. (3).

$$\text{degradation rate} = 100\% \times \frac{(C_0 - C)}{C_0} \tag{3}$$

Here, C_0 is the initial concentration of MB before UV irradiation, and C is the concentration of MB remaining in the solution, and the apparent first-order kinetic equation (Eq. (4)) was used to fit the experimental data:

$$\ln\left(\frac{C_0}{C}\right) = k_{app} \times t \tag{4}$$

where k_{app} is the apparent reaction rate constant, and t is the reaction time [28]. For comparison, the same procedure was also performed for TiO_2 hollow spheres.

3. Results and discussion

3.1. Characterization of WO_3/TiO_2 composites

3.1.1. Morphology

Composite photocatalyst WO_3/TiO_2 hollow spheres were synthesized using a colloidal carbon template. The micrographs of the samples were observed by SEM and TEM. Fig. 1 shows the SEM and TEM images of the carbon sphere template obtained by hydrothermal synthesis. The micrographs of the carbon spheres showed that

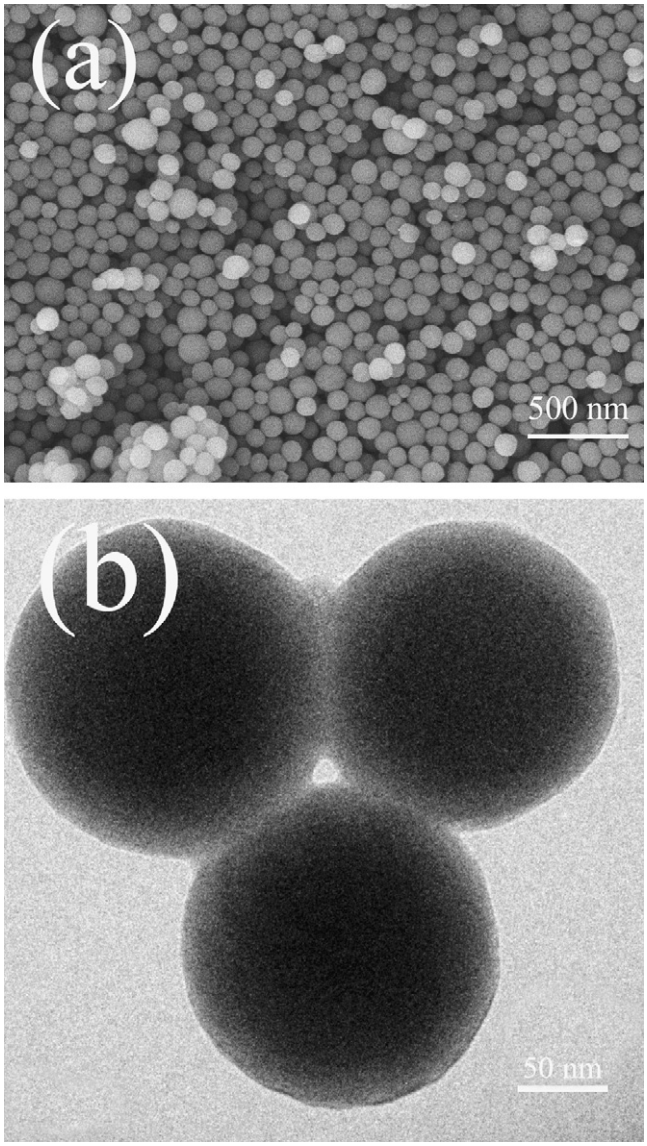

Fig. 1. (a) SEM and (b) TEM images of carbon spheres.

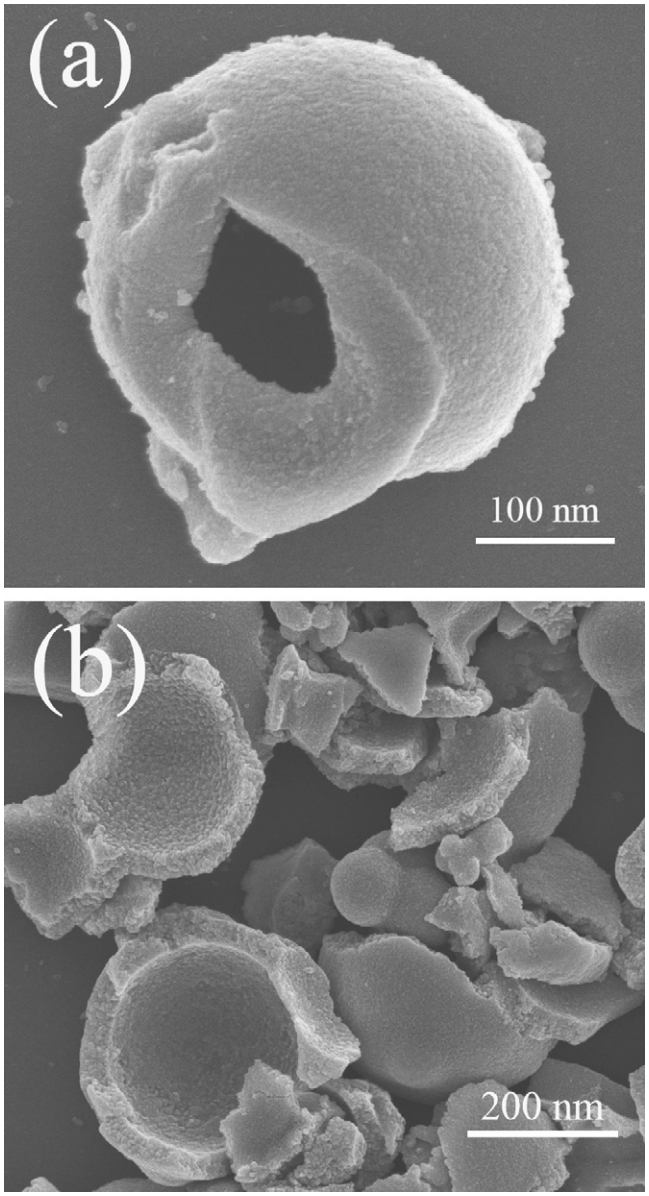

Fig. 2. SEM images of WO_3/TiO_2 spheres (a) without ultrasound and (b) with ultrasound.

the carbon balls were nearly mono-dispersed, spherical structures with uniform particle size distributions. In addition, the balls had smooth surfaces, and the diameter of the colloidal carbon spheres ranged from 180–250 nm.

Fig. 2a shows an SEM micrograph of the WO_3/TiO_2 hollow spheres obtained after the removal of the carbon sphere template. The calcinations of these composite particles resulted in the fabrication of hollow spheres. The diameter of the composite photocatalysts was about 320 nm. Ultrasound images of the composite photocatalysts are shown in Fig. 2b. The images further confirmed that the composite catalysts had a hollow spherical structure and that the wall thickness of the WO_3/TiO_2 hollow spheres was about 50 nm.

3.1.2. Phases

XRD was used to characterize the crystalline phases of the photocatalysts. XRD patterns of the WO_3/TiO_2 phases formed at 550 °C are shown in Fig. 3. The presence of five main peaks of TiO_2 at $2\theta = 25.22°$, 37.78°, 47.94°, 54.96°, and 62.69° were found; these peaks can be respectively indexed to the (101), (004), (200), (211), and (204) planes of anatase titanium. The patterns clearly indicated that the nanoparticles had a pure anatase structure, with

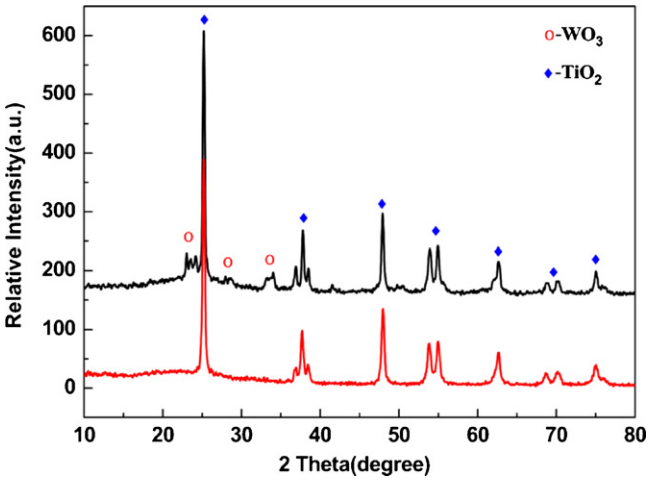

Fig. 3. XRD patterns of WO_3/TiO_2 and TiO_2 hollow spheres.

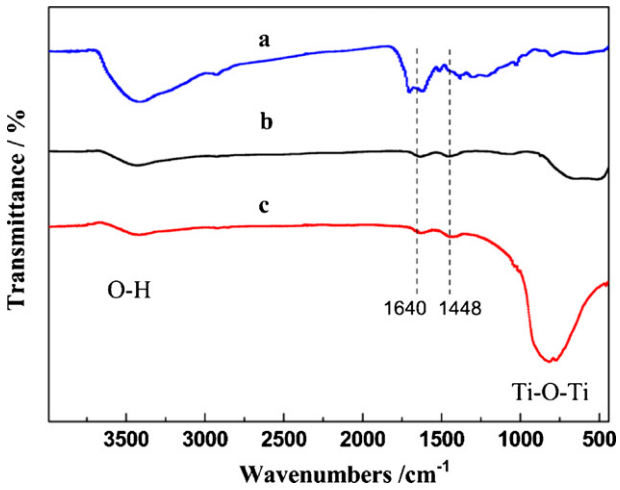

Fig. 4. FT-IR spectra of (a) carbon sphere template, (b) TiO_2, and (c) WO_3/TiO_2 hollow spheres.

all major peaks matching well with the standard pattern of anatase titanium (JCPDS no. 21-1272). The crystallite size, calculated by the Scherrer formula (Eq. (1)), was 32 nm. No characteristic carbon peak was found, indicating that the carbon sphere template was completely removed at 550 °C.

3.1.3. FT-IR

The FT-IR spectra of the WO_3/TiO_2 hollow spheres and TiO_2 are shown in Fig. 4. The characteristic absorption band at ~3420 cm^{-1} was attributed to –OH stretching, that at ~1630 cm^{-1} was attributed to aromatic and –OH bending vibrations, and that at ~1448 cm^{-1} was attributed to C–H stretching vibrations. All of the samples showed relatively intense and broad bands in the vicinity of 400–800 cm^{-1} due to Ti–O vibrations [29]. No characteristic peak of CO_2 was found at ~2370 cm^{-1}, confirming the successful removal of the carbon spheres.

Based on the study by Wang et al. [30–32], we proposed a generating mechanism for the fabrication of WO_3/TiO_2 hollow spheres by templating carbonaceous microspheres as illustrated in Fig. 5. Carbon microspheres, which served as the templates, were first prepared from glucose by dehydration under hydrothermal conditions. According to researches done by Sun and Li [26], the surface of the spheres is hydrophilic, as it is functionalized with –OH and C=O groups, which is illustrated in Fig. 5a. Upon dispersal of the carbon microspheres in $Ti(OBu)_4$ and ammonium metatungstate, the functional groups in the surface layer were able to bind metal cations (such as Ti^{2+} species formed in the reaction media during the hydrolysis of $Ti(OBu)_4$ salts) through coordination or electrostatic interactions. The formation process can be seen in Fig. 5b. After the removal of carbon templates by calcination, the hollow spheres achieved an average diameter of about 320 nm, roughly 50 nm larger than the starting spheres.

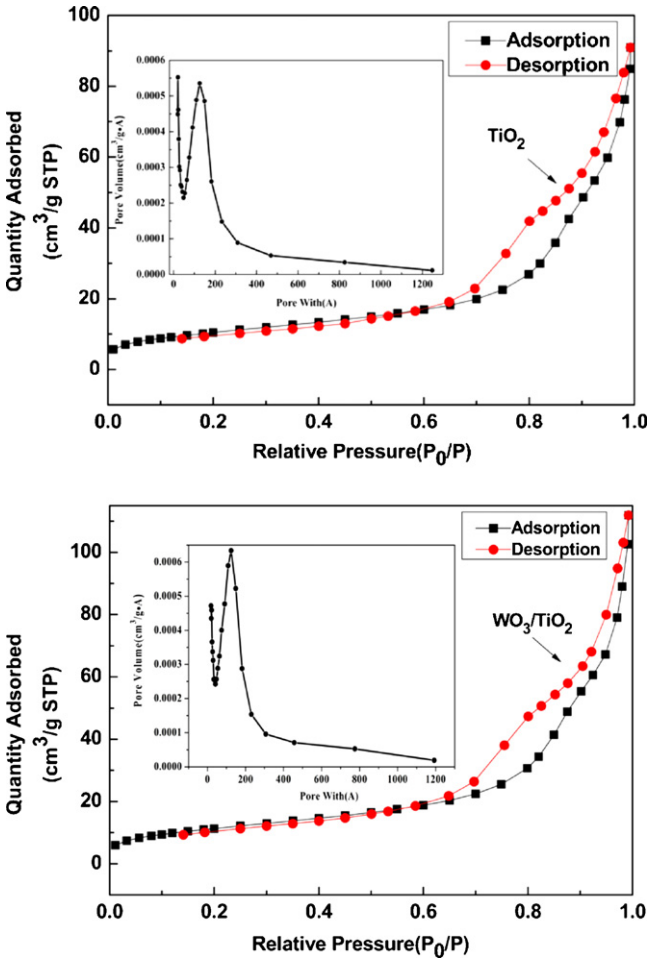

Fig. 6. Nitrogen adsorption–desorption isotherm of WO_3/TiO_2 and TiO_2 hollow spheres (inset: pore size distribution curves).

3.1.4. BET

To characterize the specific surface area and porosity of the as-prepared samples, N_2 adsorption analysis was carried out. Fig. 6 shows the N_2 adsorption–desorption isotherms and the corresponding pore-size distribution curves of the two titania samples. The isotherms corresponding to the WO_3/TiO_2 and TiO_2 hollow spheres were of type IV, according to Brunauer–Deming–Deming–Teller (BDDT) classification. Two capillary condensation steps were found, indicating bimodal pore-size distributions in the mesoporous (pore diameters between 2 and 50 nm) and macroporous (pore diameters larger than 50 nm) regions [33]. The hysteresis loop at lower relative pressure ranges ($0.4 < P/P_0 < 0.9$) was associated with finer intra-aggregated pores within primary agglomerated particles, while that at higher relative pressure ranges ($0.9 < P/P_0 < 1$) was related to larger inter-

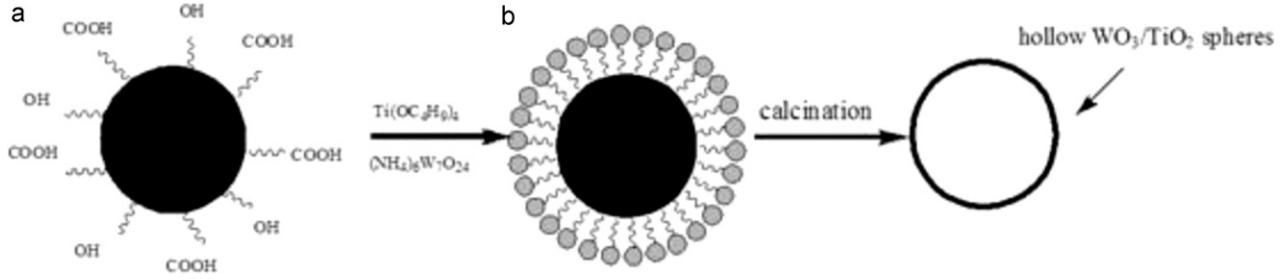

Fig. 5. Schematic of the formation of WO_3/TiO_2 hollow spheres using carbon spheres as a template.

Table 1
Surface area, pore volume, and average pore size of WO_3/TiO_2 and TiO_2 hollow spheres.

Sample	S_{BET} ($m^2\ g^{-1}$)	V_{tot} ($cm^3\ g^{-1}$)	D (nm)
TiO_2	37.52	0.1408	15.01
WO_3/TiO_2	40.95	0.1735	16.91

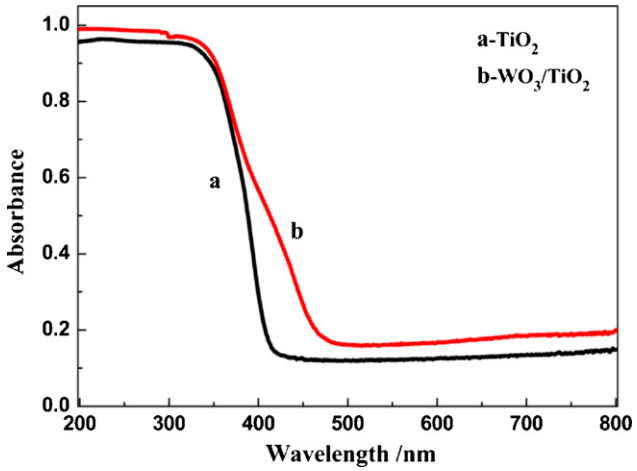

Fig. 7. Diffuse reflectance UV–vis spectra of WO_3/TiO_2 and TiO_2 hollow spheres.

aggregated pores between secondary aggregated particles [34]. This bimodal pore-size distribution was confirmed by the corresponding pore-size distributions (see inset in Fig. 6). A relative pressures approaching unity, the adsorption isotherm was similar to a type II isotherm curve, indicating the presence of mesopores among the agglomerated WO_3/TiO_2 hollow spheres. The tailing of the pore-size distribution curve showed the presence of macro pores [34,35]. The specific surface area, pore volume, and average pore size of the WO_3/TiO_2 and TiO_2 hollow spheres are shown in Table 1. It can be seen that the WO_3/TiO_2 hollow spheres had relatively higher surface-to-volume ratios compared to TiO_2 ones.

3.1.5. Absorption spectrum

The UV–vis diffuse reflectance spectrum of TiO_2 is shown in Fig. 7a. It was dominated by the edge due to the O^{2-}–Ti^{4+} charge transition in anatase TiO_2 at 300–380 nm [36,37], which is comparable to the excitation of electrons from the valence band to the conduction band.

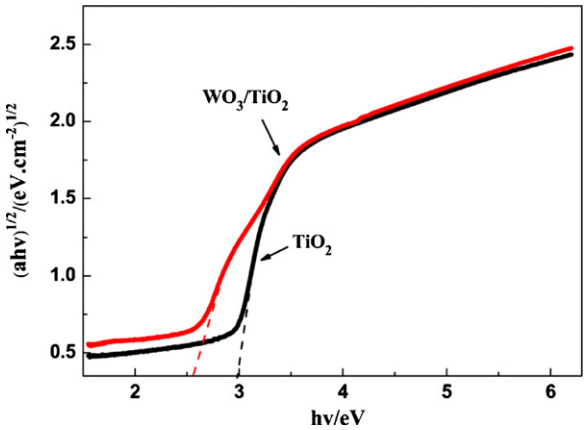

Fig. 8. Plots of $(ahv)^{1/2}$ versus photon energy (hv) of WO_3/TiO_2 and TiO_2 hollow spheres.

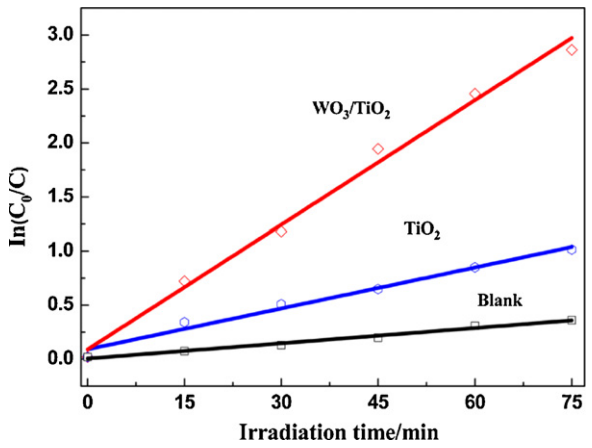

Fig. 9. Linear transform $\ln(C_0/C) = f(t)$ of the kinetic curves of MB degradation of WO_3/TiO_2 and TiO_2 hollow spheres under UV irradiation.

In Fig. 7b, the main absorption edge of the WO_3/TiO_2 hollow spheres was 477 nm, which was shifted towards the visible region compared to pure TiO_2. As well, the absorption of WO_3/TiO_2 was stronger than that of TiO_2 in the visible region. The plots of $(ahv)^{1/2}$ versus hv are presented in Fig. 8. The indirect band gap energies estimated from the intercept of the tangents to the plots were 3.0 and 2.6 eV for TiO_2 and WO_3/TiO_2 hollow spheres, respectively. Therefore, the light-harvesting efficiency of WO_3/TiO_2 hollow spheres was larger than that of TiO_2 ones.

The red-shift in the absorption spectrum of the WO_3/TiO_2 hollow spheres may be attributed to two reasons. First, the indirect band gap energy of anatase titania was 3.2 eV; it was 2.8 eV for WO_3. When WO_3 and TiO_2 form a coupled photocatalyst, the formation of defective energy levels within the forbidden band of WO_3 and TiO_2 could decrease the band gap energy of WO_3/TiO_2 [18,38]. Second, oxygen defects that occurred during the formation of titania particles may have caused the spheres to red-shift. Oxygen defects would extend titanic activity to the visible region; this phenomenon was investigated by Martyanov et al. [39].

3.2. Photocatalytic application of WO_3/TiO_2

Evaluation of the photocatalytic activities of WO_3/TiO_2 and TiO_2 hollow spheres was carried out by the degradation of MB under UV or visible light irradiation. The level of mineralization with irradi-

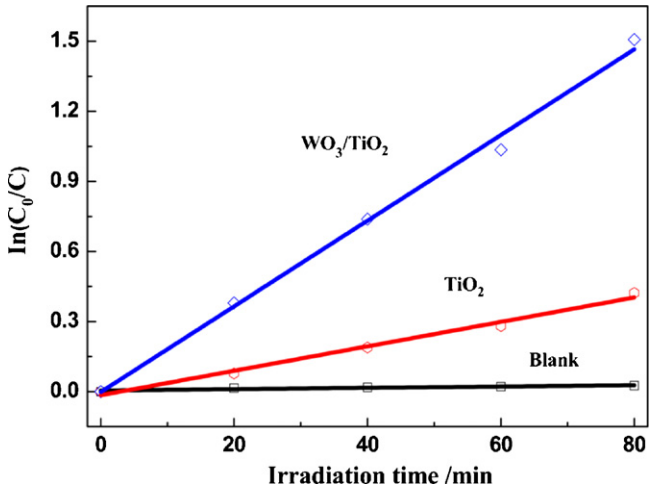

Fig. 10. Linear transform $\ln(C_0/C) = f(t)$ of the kinetic curves of MB degradation of WO_3/TiO_2 and TiO_2 hollow spheres under visible light irradiation.

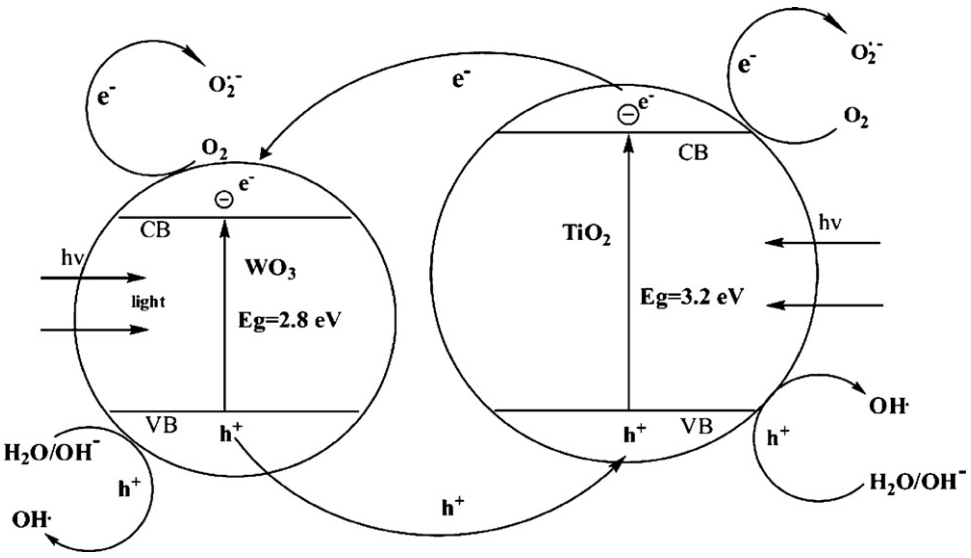

Fig. 11. Schematic representation of charge carrier separation in the photoexcited WO_3/TiO_2 photocatalyst.

ation time was investigated by analyzing the UV–visible spectra of the reaction solution obtained at 5 and 15 min intervals. Fig. 9 shows the results of the photocatalytic decomposition of MB under UV irradiation. After 60 min irradiation, the degradation rate (Eq. (3)) of MB was 95%, 57%, and 30% for WO_3/TiO_2 hollow spheres, TiO_2 hollow spheres, and blank hollow spheres without catalysts, respectively. This shows that WO_3-loaded TiO_2 had enhanced photocatalytic activity, and the linear relationship between $\ln(C_0/C)$ and t indicates that the photo-catalytic degradation reaction follows pseudo-first-order kinetics (Fig. 9). From Fig. 9, we obtained the following k_{app} data for WO_3/TiO_2 and TiO_2 hollow spheres: 0.041 and 0.013 min^{-1}, respectively. The correlation coefficients R^2 were 0.99 and 0.98 for WO_3/TiO_2 and TiO_2 hollow spheres, respectively.

Fig. 10 shows the photocatalytic properties of the TiO_2 and WO_3/TiO_2 hollow spheres under visible light irradiation. The blank test confirmed that MB only slightly degraded under visible light in the absence of catalysts, indicating that the photolysis and adsorption action of catalysts can be ignored. Only 24% MB can be photodegraded by TiO_2 under visible light in 80 min. The sample with WO_3 exhibited higher photocatalytic activity than pure TiO_2. 78% of MB can be photodegraded by WO_3/TiO_2 under the same condition. Meanwhile, the linear relationship between $\ln(C_0/C)$ and t indicates that the photo-catalytic degradation reaction also follows pseudo-first-order kinetics (Fig. 10). On the basis of the pseudo-first-order reaction, the apparent rate constants were calculated to be 0.00524, 0.0184, and 0.000283 min^{-1} for pure TiO_2, WO_3/TiO_2 and bank hollow spheres without catalysts, respectively. Results showed that the coupled with WO_3 sample had a great influence on the photocatalytic activity of the as-prepared photocatalyst and demonstrate that fabricated mixed metal oxide hollow spheres could potentially be used as an efficient photocatalyst for degradation of organic pollutants. In comparison to the UV photoactivity, the photocatalysts showed lower apparent rate constant in the visible region (Table 2). It is worth mentioning here that the apparent rate constant in the presence of fabricated WO_3/TiO_2 hollow spheres is 3-fold higher than those reported in the literature [28]. Moreover, according to the studies by Saepurahman et al. [40–42], it is interesting to find that the optimal conditions of WO_3/TiO_2 photocatalysts with other preparation technique (hydrothermal method [21], sol–gel method [32], and flame-made method [41]) is not the same and the apparent rate constant could be improved by the procedure of preparation such as catalyst loading, optical absorption, initial PH, light wavelength, and calcination temperature [40,42].

Table 2
UV and visible apparent rate constant k (min^{-1}) for the TiO_2 and WO_3/TiO_2 hollow spheres.

Sample	k (min^{-1}) UV degradation	k (min^{-1}) visible degradation
Blank	0.005	0.00028
TiO_2	0.013	0.0052
WO_3/TiO_2	0.041	0.018

The increased photocatalytic activity of the coupled photocatalyst was primarily attributed to enhancements in charge separation efficiency because a junction [4,18,28] was formed by the decoration of WO_3 with TiO_2, which plays an important role in the separation of photogenerated electron–hole pairs (Fig. 11).

When WO_3 (E_g = 2.8 eV) and TiO_2 (E_g = 3.2 eV) form a coupled photocatalyst, WO_3 can be excited by photons under visible illumination, and TiO_2 remain unexcited. Upon visible excitation, an electron from the anatase TiO_2 and WO_3 may be promoted from the valence band (e_{cb}^-) to the conduction band, leaving behind a hole in the valence band (h_{VB}^+). As the conduction band of WO_3 is lower than that of TiO_2, the former can be used as a photoelectronic receiver. The photo-generated electrons of the TiO_2 conduction band will be transferred to the conduction band of WO_3 [20]. Since the holes move in the opposite direction from the electrons, photogenerated holes will be trapped within the TiO_2 particle, causing charge separation to become more efficient [21,41]. The positive holes in the valence band can be trapped by OH^- or H_2O species adsorbed on the surface of the catalyst, producing reactive hydroxyl radicals in aqueous media. The photo-generated electrons accumulate on the surface of WO_3 and could be rapidly transferred to molecular oxygen O_2 to form the superoxide radical anion $O_2^{\bullet -}$ and hydrogen peroxide H_2O_2 [18,21]. The newly formed intermediates can interact to produce a hydroxyl radical $OH^{\bullet}$, which is responsible for the decomposition of MB.

4. Conclusions

Hollow spheres composed of WO_3/TiO_2 mixed metal oxide shells were fabricated by the template method. The as-synthetic hollow spheres exhibited high catalytic activity for MB photo-

degradation under visible light irradiation. The indirect band gap energies of TiO_2 and WO_3/TiO_2 hollow spheres were 3.0 and 2.6 eV, respectively. WO_3-loaded TiO_2 can shift the light absorption band from near UV to the visible region. Kinetic studies indicated that the photocatalytic degradation of MB followed pseudo-first-order kinetics. The photocatalytic mineralization of MB, catalyzed by TiO_2 or WO_3/TiO_2 proceeded at a significantly higher rate under UV irradiation than that under visible light. The apparent rate constant of photodestruction of MB catalyzed by WO_3/TiO_2 composite semiconductor material was 3.2 and 3.5-fold higher than by TiO_2 under both UV and visible light irradiation. The increased photocatalytic activity of the coupled nanocomposites was attributed to photoelectron/hole separation efficiency and the extension of the wavelength range of photoexcitation.

Acknowledgments

This research was supported by a grant from Planned Science and Technology Project of Hunan Province, China (no. 2008SK1001). This study was also partly supported by the State Key Program of National Natural Science Foundation of China (no. 51072232). Here, we are grateful for their financial supports.

References

[1] A. Fujishima, T.N. Rao, D.A. Tryk, Titanium dioxide photocatalysis, J. Photochem. Photobiol. C 1 (2000) 1–21.
[2] E.J. Wolfrum, J. Huang, D.M. Blake, P.C. Maness, Z. Huang, J. Fiest, W.A. Jacoby, Photocatalytic oxidation of bacteria, bacterial and fungal spores, and model biofilm components to carbon dioxide on titanium dioxide-coated surfaces, Environ. Sci. Technol. 36 (2002) 3412–3419.
[3] M.R. Hoffmann, S.T. Martin, W.Y. Choi, D.W. Bahnemann, Environmental applications of semiconductor photocatalysis, Chem. Rev. 95 (1995) 69–96.
[4] M. Asiltürk, F. Sayılkan, E. Arpac, Effect of Fe^{3+} ion doping to TiO_2 on the photocatalytic degradation of Malachite Green dye under UV and vis-irradiation, J. Photochem. Photobiol. A 203 (2009) 64–71.
[5] M. Andersson, L. Osterlund, S. Ljungstrom, A. Palmqvist, Preparation of nanosize anatase and rutile TiO_2 by hydrothermal treatment of microemulsions and their activity for photocatalytic wet oxidation of phenol, J. Phys. Chem. B 106 (2002) 10674–10679.
[6] H. Tada, A. Hattori, Y. Tokihisa, K. Imai, N. Tohge, S. Ito, A patterned-TiO_2/SnO_2 bilayer type photocatalyst, J. Phys. Chem. B 104 (2000) 4585–4587.
[7] J.G. Yu, W. Liu, H.G. Yu, A one-pot approach to hierarchically nanoporous titania hollow microspheres with high photocatalytic activity, Cryst. Growth Des. 8 (2008) 930–934.
[8] S.H. Woo, W.W. Kim, S.J. Kim, C.K. Rhee, Photocatalytic behaviors of transition metal ion doped TiO_2 powder synthesized by mechanical alloying, Mater. Sci. Eng., A 449 (2007) 1151–1154.
[9] N. Sobana, M. Muruganadham, M. Swaminathan, Nano-Ag particles doped TiO_2 for efficient photodegradation of direct azo dyes, J. Mol. Catal. A: Chem. 258 (2006) 124–132.
[10] S. Alex, U. Santhosh, S. Das, Dye sensitization of nanocrystalline TiO_2: enhanced efficiency of unsymmetrical versus symmetrical squaraine dyes, J. Photochem. Photobiol. A 172 (2005) 63–71.
[11] Z.X. Zhou, S.P. Qian, S.D. Yao, Z.Y. Zhang, Photosensitization of a colloidal TiO_2 semiconductor system with hypocrellin B, Dyes Pigm. 51 (2001) 137–144.
[12] J.T. Tian, L.J. Chen, Y.S. Yin, X. Wang, J.H. Dai, Z.B. Zhu, X.Y. Liu, P.W. Wu, Photocatalyst of TiO_2/ZnO nano composite film: preparation, characterization, and photodegradation activity of methyl orange, Surf. Coat. Technol. 204 (2009) 205–214.
[13] K.S. Chung, Z. Jiang, B.S. Gill, J.S. Chung, Oxidative decomposition of o-dichlorobenzene over V_2O_5/TiO_2 catalyst washcoated onto wire-mesh honeycombs, Appl. Catal. A 237 (2002) 81–89.
[14] D. Das, H.K. Mishra, K.M. Parida, A.K. Dalai, Preparation, physico-chemical characterization and catalytic activity of sulphated ZrO_2–TiO_2 mixed oxides, J. Mol. Catal. A: Chem. 189 (2002) 271–282.
[15] A. Kitiyanan, S. Sakulkhaemaruethai, Y. Suzuki, S. Yoshikawa, Structural and photovoltaic properties of binary TiO_2–ZrO_2 oxides system prepared by sol-gel method, Compos. Sci. Technol. 66 (2006) 1259–1265.
[16] M.G. Kang, H.E. Han, K.J. Kim, Enhanced photodecomposition of 4-chlorophenol in aqueous solution by deposition of CdS on TiO_2, J. Photochem. Photobiol. A 125 (1999) 119–125.
[17] J.C. Tristo, F. Magalhaes, P. Corio, M.T.C. Sansiviero, Electronic characterization and photocatalytic properties of CdS/TiO_2 semiconductor composite, J. Photochem. Photobiol. A 181 (2006) 152–157.
[18] V. Iliev, D. Tomova, S. Rakovsky, A. Eliyas, G.L. Puma, Enhancement of photocatalytic oxidation of oxalic acid by gold modified WO_3/TiO_2 photocatalysts under UV and visible light irradiation, J. Mol. Catal. A: Chem. 327 (2010) 51–57.
[19] V. Puddu, R. Mokaya, G.L. Puma, Novel one step hydrothermal synthesis of TiO_2/WO_3 nanocomposites with enhanced photocatalytic activity, Chem. Commun. 2007 (2007) 4749–4751.
[20] V. Keller, P. Bernhardt, F. Garin, Photocatalytic oxidation of butyl acetate in vapor phase on TiO_2, Pt/TiO_2 and WO_3/TiO_2 catalysts, J. Catal. 215 (2003) 129–138.
[21] X.Z. Li, F.B. Li, C.L. Yang, W.K. Ge, Photocatalytic activity of WO_x–TiO_2 under visible light irradiation, J. Photochem. Photobiol. A 141 (2001) 209–217.
[22] N. Serpone, P. Maruthamuthu, P. Pichat, E. Pelizzetti, H. Hidaka, Exploiting the interparticle electron transfer process in the photocatalysed oxidation of phenol, 2-chlorophenol and pentachlorophenol: chemical evidence for electron and hole transfer between coupled semiconductors, J. Photochem. Photobiol. A. 85 (1995) 247–255.
[23] S. Guo, Z.B. Wu, H.Q. Wang, F. Dong, Synthesis of mesoporous TiO_2 nanorods via a mild template-free sonochemical route and their photocatalytic performances, Catal. Commun. 10 (2009) 1766–1770.
[24] Q.F. Chen, D. Jiang, W.M. Shi, D. Wu, Y. Xu, Visible-light-activated Ce–Si co-doped TiO_2 photocatalyst, Appl. Surf. Sci. 255 (2009) 7918–7924.
[25] L.M. Zhang, W.C. Lu, R.R. Cui, S.S. Shen, One-pot template-free synthesis of mesoporous boehmite core–shell and hollow spheres by a simple solvothermal route, Mater. Res. Bull. 45 (2010) 429–436.
[26] X. Sun, Y. Li, Colloidal carbon spheres and their core/shell structures with noble-metal nanoparticles, Angew. Chem., Int. Ed. 43 (2004) 597–601.
[27] M.H. Zhou, J.G. Yu, Preparation and enhanced daylight-induced photocatalytic activity of C, N, S-tridoped titanium dioxide powders, J. Hazard. Mater. 152 (2008) 1229–1236.
[28] J. Matos, J. Laine, J.M. Herrmann, Synergy effect in the photocatalytic degradation of phenol on a suspended mixture of titania and activated carbon, Appl. Catal. B. 18 (1998) 281–291.
[29] Y.X. Hu, J.P. Ge, Y.G. Sun, T.R. Zhang, Y.D. Yin, A self-templated approach to TiO_2 microcapsules, Nano Lett. 7 (2007) 1832–1836.
[30] H.Q. Wang, Z.B. Wu, Y. Liu, A simple two-step template approach for preparing carbon-doped mesoporous TiO_2 hollow microspheres, J. Phys. Chem. C 113 (2009) 13317–13324.
[31] X.X. Li, Y.J. Xiong, Z.Q. Li, Y. Xie, Large-scale fabrication of TiO_2 hierarchical hollow spheres, Inorg. Chem. 45 (2006) 3493–3495.
[32] X.Z. Li, F. Chen, X.W. Lu, C.Y. Ni, X.B. Zhao, Z.G. Chen, Layer-by-layer synthesis of hollow spherical CeO_2 templated by carbon spheres, J. Porous Mater. 17 (2010) 297–303.
[33] A.F. Zhang, Y.C. Zhang, N. Xing, K.K. Hou, X.W. Guo, Hollow silica spheres with a novel mesoporous shell perforated vertically by hexagonally arrayed cylindrical nanochannels, Chem. Mater. 21 (2009) 4122–4126.
[34] J.G. Yu, G.H. Wang, B. Cheng, M.H. Zhou, Effects of hydrothermal temperature and time on the photocatalytic activity and microstructures of bimodal mesoporous TiO_2 powders, Appl. Catal. B. 69 (2007) 171–180.
[35] X.X. Yu, J.G. Yu, B. Cheng, M. Jaroniec, Synthesis of hierarchical flower-like AlOOH and TiO_2/AlOOH superstructures and their enhanced photocatalytic properties, J. Phys. Chem. C 113 (2009) 17527–17535.
[36] D.N. Ke, H.J. Liu, T.Y. Peng, X. Liu, K. Dai, Preparation and photocatalytic activity of WO_3/TiO_2 nanocomposite particles, Mater. Lett. 62 (2008) 447–450.
[37] M.W. Xiao, L.S. Wang, X.J. Huang, Y.D. Wu, Z. Dang, Synthesis and characterization of WO_3/titanate nanotubes nanocomposite with enhanced photocatalytic properties, J. Alloys Compd. 470 (2009) 486–491.
[38] C.K. Xu, R. Killmeyer, L.M. Gray, S.U.M. Khan, Photocatalytic effect of carbon-modified n-TiO_2 nanoparticles under visible light illumination, Appl. Catal. B. 64 (2006) 312–317.
[39] I.N. Martyanov, S. Uma, S. Rodrigues, K.J. Klabunde, Structural defects cause TiO_2-based photocatalysts to be active in visible light, Chem. Commun. 2004 (2004) 2476–2477.
[40] Saepurahman, M.A. Abdullah, F.K. Chong, Dual-effects of adsorption and photodegradation of methylene blue by tungsten-loaded titanium dioxide, Chem. Eng. J. 158 (2010) 418–425.
[41] K.K. Akurati, A. Vital, J.P. Dellemann, K. Michalow, T. Graule, D. Ferri, A. Baiker, Flame-made WO_3/TiO_2 nanoparticles: Relation between surface acidity, structure and photocatalytic activity, Appl. Catal. B. 79 (2008) 53–62.
[42] Saepurahman, M.A. Abdullah, F.K. Chong, Preparation and characterization of tungsten-loaded titanium dioxide photocatalyst for enhanced dye degradation, J. Hazard. Mater. 176 (2010) 451–558.